ACS Catalysis

Research Article

pubs.acs.org/acscatalysis

Polymeric g-C_3N_4 Coupled with $NaNbO_3$ Nanowires toward Enhanced Photocatalytic Reduction of CO_2 into Renewable Fuel

Haifeng Shi,*[,†,‡] Guoqing Chen,[†] Chengliang Zhang,[†] and Zhigang Zou[‡]

[†]School of science, Jiangnan University, Wuxi, P. R. China, 214122

[‡]Eco-materials and Renewable Energy Research Center (ERERC), Department of Physics, Nanjing University, Nanjing, P. R. China, 210093

Supporting Information

ABSTRACT: Visible-light-responsive g-C_3N_4/$NaNbO_3$ nanowires photocatalysts were fabricated by introducing polymeric g-C_3N_4 on $NaNbO_3$ nanowires. The microscopic mechanisms of interface interaction, charge transfer and separation, as well as the influence on the photocatalytic activity of g-C_3N_4/$NaNbO_3$ composite were systematic investigated. The high-resolution transmission electron microscopy (HR-TEM) revealed that an intimate interface between C_3N_4 and $NaNbO_3$ nanowires formed in the g-C_3N_4/$NaNbO_3$ heterojunctions. The photocatalytic performance of photocatalysts was evaluated for CO_2 reduction under visible-light illumination. Significantly, the activity of g-C_3N_4/$NaNbO_3$ composite photocatalyst for photoreduction of CO_2 was higher than that of either single-phase g-C_3N_4 or $NaNbO_3$. Such a remarkable enhancement of photocatalytic activity was mainly ascribed to the improved separation and transfer of photogenerated electron−hole pairs at the intimate interface of g-C_3N_4/$NaNbO_3$ heterojunctions, which originated from the well-aligned overlapping band structures of C_3N_4 and $NaNbO_3$.

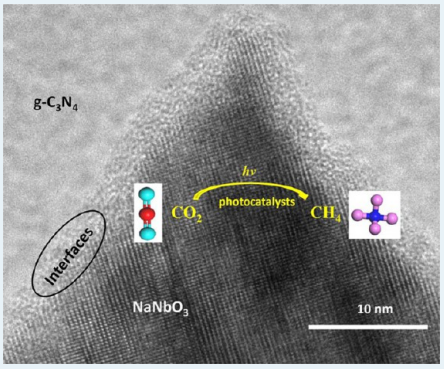

KEYWORDS: *sodium niobate, composite photocatalysts, g-C_3N_4, CO_2 conversion, nanowires*

1. INTRODUCTION

The rapidly increasing carbon dioxide (CO_2) emission in the atmosphere is becoming a more and more urgent issue in view of serious environmental problems, such as the "greenhouse effect." In addition to carbon capture and sequestration (CCS) technology,[1] the development of an artificial photosynthetic system is a promising strategy to mimic the natural photosynthetic cycle of the chemical conversion of CO_2 into a fuel or other useful chemicals. Although the reduction of CO_2 is quite challenging owing to its relatively inert and stable properties, the photocatalytic reduction of CO_2 into fuel (such as methanol or methane) using sunlight and photocatalysts at room temperature and ambient pressure appears to be a promising methodology to meet this challenge since it could alleviate the greenhouse effect as well as obtain organic fuel or basic chemical raw materials.[2−8] Actually, ever since the first report on photocatalytic reduction of CO_2 into organic compounds (formaldehyde, formic acid, methanol, and methane) over suspending TiO_2 particles in 1979,[9] many efforts have been attempted to develop highly efficient photocatalysts for CO_2 conversion in liquid or gas phase.[10−15] Unfortunately, the solar-to-chemical energy conversion efficiencies of the reported photocatalysts are still too low to make these systems commercially viable.

Over the past three decades, the development of photocatalysts for CO_2 reduction has primarily focused upon large band gap metal oxides involving ions with filled or empty d-shell bonding configurations (i.e., Ti^{4+}, Nb^{5+}, Ta^{5+}, W^{6+}, Ga^{3+}, In^{3+}, and Ge^{4+}).[16−25] Recently, a metal-free photocatalyst, polymeric graphitic carbon nitride (g-C_3N_4) with high thermal and chemical stability, has gained a great deal of scientific interest owing to its applications in photocatalytic splitting of water, organic pollutant degradation, and CO_2 reduction[26−32] since the first discovery about its photocatalytic activity for hydrogen production from water under visible light illumination.[33] However, the photocatalytic reactions over g-C_3N_4 still suffer from low conversion efficiencies due to the rapid electron−hole recombination, which is usually considered as a major barrier in the single-component semiconductor photocatalyst.

Among the various methods to improve the photocatalytic performance, the manipulation of semiconductor heterojunctions by combining two different catalysts with suitable conduction and valence bands is generally considered as one of the effective methods to prevent the photogenerated charge recombination and thereby promote the photocatalytic efficiency. Considering the benefits of composite heterojunctions, several g-C_3N_4-based composite photocatalysts, such as g-C_3N_4/ TaON,[34] g-C_3N_4/$ZnWO_4$,[35] g-C_3N_4/ZnO,[36] C_3N_4/$BiPO_4$,[37] g-C_3N_4/CdS,[38] g-C_3N_4/Bi_2WO_6,[39] g-C_3N_4/N-TiO_2,[40] and g-C_3N_4/N-$NaNbO_3$,[41] have been successfully developed and displayed significantly higher photocatalytic

Received: June 18, 2014
Revised: August 7, 2014
Published: September 17, 2014

   dx.doi.org/10.1021/cs500848f | ACS Catal. 2014, 4, 3637−3643

activity than that of the pristine material comprising the composites, which has been demonstrated in the photodegradation of organic pollutants and water splitting. However, to the best of our knowledge, there are few reports about the C_3N_4 composite photocatalysts for photocatalytic CO_2 reduction.[42,43]

Environmentally friendly sodium niobate ($NaNbO_3$) with unique crystal structures containing a network of corner-shared octahedral units of [NbO_6], which is helpful for enhancing the charge migration in the crystals, was recently reported as an efficient photocatalyst for water splitting and CO_2 reduction.[44−49] Unfortunately, the relative wide band gap (3.4 eV) limits its photocatalytic activity only to be active in the ultraviolet light region (4% of the solar spectrum). Considering the efficient utilization of the visible light (43% of the total sunlight) to generate electron−hole pairs for promoting photocatalytic redox reactions, therefore, it is highly desirable to develop a photocatalyst with an efficient response under visible-light irradiation. Currently, one-dimensional nanowire materials have attracted extraordinary attention for promising application in photocatalysis because nanowire photocatalysts generally provide larger surface-to-volume ratios and possess more efficient ballistic charge transport along the single nanowires than the diffusive transport in powdered materials.[50,51] In our previous work, we have successfully synthesized $NaNbO_3$ nanowires with excellent performance in both photocatalytic water splitting and CO_2 reduction.

Herein, in this study, the g-C_3N_4/$NaNbO_3$ nanowire composite photocatalysts were prepared. The physical characteristics of samples were examined using the following techniques, such as XRD, BET measurement, FE-SEM, HRTEM, XPS, photoluminescence spectra, and UV−vis diffuse reflectance spectroscopy. Significantly, we found that the as-prepared g-C_3N_4/$NaNbO_3$ nanowire composite photocatalyst exhibited remarkably enhanced photocatalytic activity for CH_4 production yield in visible-light-driven CO_2 reduction. A possible mechanism for enhancing photocatalytic activity of g-C_3N_4/$NaNbO_3$ was also proposed in view of the interface interaction of photoinduced carrying transfer and separation.

2. EXPERIMENTAL SECTION

2.1. Catalyst Synthesis. As for the preparation of $NaNbO_3$ nanowires, we first synthesized $Na_2Nb_2O_6{\cdot}H_2O$ nanowires via a facile hydrothermal route and then converted the precursors into $NaNbO_3$ with similar nanostructures through a heat process, which is in accord with a previous report.[48] In a typical case, 1 g of P123 ($EO_{20}PO_{70}EO_{20}$, BASF, USA) was first added to 25 mL of distilled water under continuous stirring at 40 °C for 2 h, followed by the addition of 5 g of $Nb(OC_2H_5)_5$ (Aldrich, USA). Subsequently, NaOH (Wako, Japan) solution (20 mol L^{-1}, 10 mL) was added drop by drop into the above solution. After being stirred for 1 h at 40 °C, the so-obtained suspension was transferred into a Teflon-lined autoclave and thermally treated at 200 °C for 24 h. The so-obtained white precipitate was washed with distilled water and ethanol and subsequently dried in an oven at 70 °C overnight. The so-obtained precursors were heated at 550 °C for 4 h to synthesize the $NaNbO_3$ orthorhombic phase nanowires. The typical preparation of g-C_3N_4/$NaNbO_3$ photocatalysts was as follows: $NaNbO_3$ nanowires and melamine powder with mass ratio of 1:4 were added into a mortar and then ground for 30 min using a pestle. The mixed powder was added and pressed into a crucible and then heated at 520 °C in a muffle furnace for 4 h with a heating rate of 20 °C min^{-1}. The final composite g-C_3N_4/$NaNbO_3$ photocatalysts were obtained. Pure g-C_3N_4 was prepared by heating melamine in the air at 520 °C for 4 h. The Pt loading on photocatalysts was synthesized using an in situ photodeposition method. Typically, 0.1 g of photocatalyst, 40 mL of distilled water, 15 mL of CH_3OH, and a given amount of $H_2PtCl_6{\cdot}6H_2O$ (0.5%) were placed in a glass vessel. The reactant solution was irradiated with a 300W Xe arc lamp for 8 h with constant stirring. Then the Pt-loaded photocatalysts were filtered and washed thoroughly with deionized water and alcohol, subsequently dried at 60 °C for 12h.

2.2. Sample Characterization. The crystal structures of samples were measured with a powder X-ray diffractometer (DX2700, Haoyuan Instrument Co., Ltd., Dandong, China) with Cu Kα radiation in the 2θ range of 10−80°. The diffuse reflectance spectra of the sample were conducted in the range of 250−850 nm using a UV−vis spectrophotometer (UV-2600; Shimadzu, Japan) equipped with an integrating sphere attachment. The absorption spectra were transformed according to the Kubelka−Munk relation, $K/S = (1 - R)^2/2R$, where R means the value of reflectance measurements and K and S are the absorption and scattering coefficients of the sample, respectively. Morphologies of samples were characterized by a field-emission scanning electron microscope (FE-SEM; FEI Tecnai G2 F30, USA) and a high resolution transmission electron microscope (HRTEM, JEM-2010, operated at 200 kV, JEOL, Japan). The specific surface areas were deduced according to the Brunauer−Emmett−Teller method using a surface area and porosimetry analyzer (V-sorb 2800, Gold APP, China) at 77 K. X-ray photoelectron spectroscopy (XPS) analysis was carried on a PHI 5000 versaprobe instrument (ULVAC-PHI, Chigasaki, Japan) using Al Kα monochromatic X-ray radiation. Photoluminescence (PL) spectra were measured at room temperature on a fluorescence spectrophotometer (FLS920P, Edinburgh, England) with an excitation wavelength of 350 nm.

2.3. Photocatalytic Activity Test. The photoreduction of CO_2 into CH_4 was carried out in a Pyrex glass vessel. The sample (50 mg) was uniformly and evenly dispersed on the bottom of a small glass cell that was located in the bottom of a Pyrex glass cell, which was connected with a closed system. The volume of the reaction system was about 230 mL. A 300 W xenon arc lamp was used as the light source of the photocatalytic reaction. The reaction setup was vacuum-treated several times, and then the high purity of CO_2 gas was followed into the reaction setup for reaching ambient pressure. After replacing the system air into CO_2, a total of 2 mL of H_2O was injected into the reactor with a liquid syringe. A gas pump was used to accelerate gas diffusion. Subsequently, the reactor was stored under dark conditions for 2 h to ensure that an adsorption−desorption equilibrium was reached. Finally, the reactor was irradiated from a 300-W Xe lamp quipped with a UV cutoff filter (λ > 420 nm). During irradiation, a gaseous sample (0.5 mL) was continually extracted from the reaction cell at a given interval to check the concentration of CH_4 using a gas chromatograph (GC-9790A, Fuli, China).

3. RESULTS AND DISCUSSION

3.1. Characterization of g-C_3N_4/$NaNbO_3$ Heterojunctions. The powder XRD patterns of the as-prepared g-C_3N_4, $NaNbO_3$, and g-C_3N_4/$NaNbO_3$ composite samples are presented in Figure 1. The two distinct peaks located at 27.4° and 13.1° of the pure g-C_3N_4 sample could be indexed as

dx.doi.org/10.1021/cs500848f | ACS Catal. 2014, 4, 3637−3643

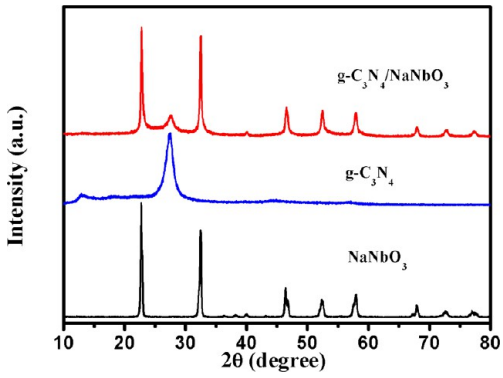

Figure 1. XRD patterns of pure $NaNbO_3$, g-C_3N_4, and g-C_3N_4/$NaNbO_3$ composite photocatalysts.

(002) and (100) diffraction planes (JCPDS 87-1526), corresponding to the characteristic interplanar staking peaks of aromatic systems and the interlayer structural packing, respectively. No impurity phase was observed in the $NaNbO_3$ sample, which was consistent with the XRD pattern of orthorhombic structured $NaNbO_3$ in the JCPDS card (no. 01-072-7753). The XRD patterns of g-C_3N_4/$NaNbO_3$ revealed coexistence peaks of $NaNbO_3$ and g-C_3N_4 in the composite. Hence the heterojunction was composed of two phases: g-C_3N_4 and $NaNbO_3$.

Figure 2 shows the UV−vis absorption spectra of $NaNbO_3$, g-C_3N_4, and g-C_3N_4/$NaNbO_3$, which are transformed from the

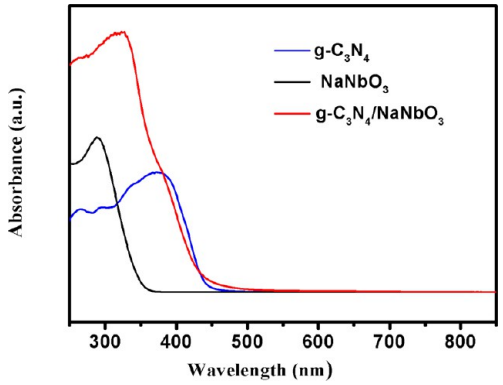

Figure 2. UV−vis diffuse reflectance spectra of pure $NaNbO_3$, g-C_3N_4, and g-C_3N_4/$NaNbO_3$ composite photocatalysts.

diffuse reflection spectra according to the Kubelka−Munk theory. The absorbance threshold of $NaNbO_3$ was located at approximately 365 nm, whereas the g-C_3N_4 sample could absorb solar energy with a wavelength up to 450 nm. The band gaps of photocatalysts were generally obtained according to the relationship $E_g = 1240/\lambda$, where E_g is the band gap energy and λ is the cutoff wavelength of the photocatalyst. Thus, the band gaps of as-prepared $NaNbO_3$ and g-C_3N_4 were determined to be 3.4 and 2.7 eV, respectively, which were consistent with the values in previous reports.[33,48] The g-C_3N_4/$NaNbO_3$ composite sample exhibited a similar tail optical absorption edge up to 450 nm. This clearly demonstrated that g-C_3N_4/$NaNbO_3$ had potential applications in the visible-light region.

The morphologies and microstructures of g-C_3N_4, $NaNbO_3$, and g-C_3N_4/$NaNbO_3$ samples were investigated with field emission scanning electron microscopy (FE-SEM). Figure 3 shows the FE-SEM images of pure g-C_3N_4, $NaNbO_3$, and g-

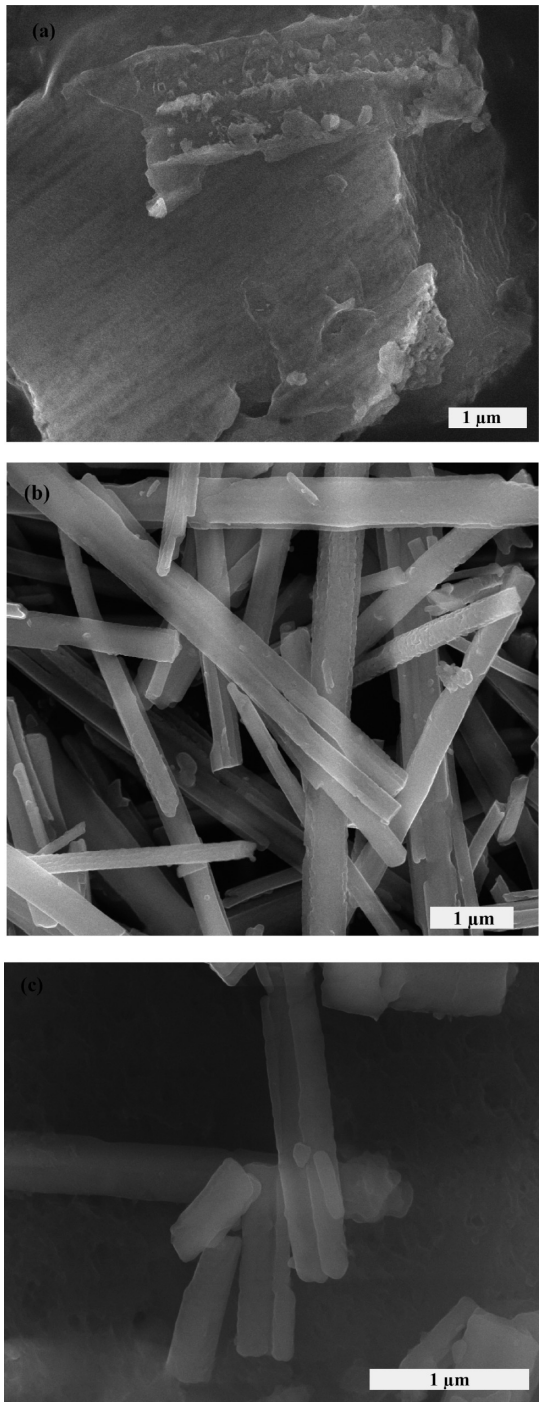

Figure 3. FE-SEM images of (a) g-C_3N_4, (b) $NaNbO_3$, and (c) g-C_3N_4/$NaNbO_3$.

C_3N_4/$NaNbO_3$ heterojunctions. It is revealed that g-C_3N_4 displays an aggregated layered structure with several stacking layers (Figure 3a). The $NaNbO_3$ sample displays a number of nanowires with a uniform diameter of ∼200 nm and length of up to several tens of micrometers (Figure 3b). As shown in Figure 3c, after introducing $NaNbO_3$, amounts of $NaNbO_3$ nanowires are found to randomly deposit and distribute on the surface of g-C_3N_4 sheets, which results in forming a heterostructured g-C_3N_4/$NaNbO_3$ material. Further EDX analysis (see Figure S1) indicates that the composite sample is composed of Na, Nb, C, N, and O atoms. Additionally, the

dx.doi.org/10.1021/cs500848f | ACS Catal. 2014, 4, 3637−3643

intensity of the nitrogen peak in Figure S1a is notably higher than that in Figure S1b, indicating that zones a and b in FE-SEM images are mainly C_3N_4 and $NaNbO_3$ nanowires, respectively.

To get further information concerning the microstructures of the g-C_3N_4/$NaNbO_3$, high-resolution transmission electron microscopy (HRTEM) analysis was performed. The low- and high-magnification transmission electron microscopy (TEM) images of the as-prepared samples are shown in Figure 4. Given the observed morphology of $NaNbO_3$ in the SEM image, the dark parts in the TEM image (Figure 4a) should be $NaNbO_3$, while the light parts correspond to C_3N_4, which further demonstrates that $NaNbO_3$ nanowires have covered the surface of C_3N_4. In addition, it is worthwhile to note that the ultrasonication treatment during the TEM preparation procedure does not peel off these nanowires (Figure 4a) owing to the strong interaction between g-C_3N_4 and $NaNbO_3$ in the heterojunctions. From the high-resolution TEM image of the g-C_3N_4/$NaNbO_3$ heterojunction (Figure 4b), smooth and intimate interfaces are obviously observed between the g-C_3N_4 and $NaNbO_3$, which confirms the formation of g-C_3N_4/$NaNbO_3$ heterojunctions. Moreover, this result also implies that g-C_3N_4/$NaNbO_3$ is heterogeneous in structure rather than a physical mixture of two separate phases of g-C_3N_4 and $NaNbO_3$. The clear lattice fringe in HRTEM (Figure 4c) should be ascribed to $NaNbO_3$, and the *d* spacing values are 0.39 and 0.27 nm, corresponding to the (101) and (002) planes of orthorhombic-structured $NaNbO_3$, respectively. The observed interface is possibly favorable for the photoinduced-carriers transfer between C_3N_4 and $NaNbO_3$ and thereby promotes the separation of photogenerated electron−hole pairs.

The surface chemical compositions and states of the g-C_3N_4, $NaNbO_3$, and g-C_3N_4/$NaNbO_3$ were further investigated by X-ray photoelectron spectroscopy (XPS) in order to clarify the interactions of $NaNbO_3$ with the g-C_3N_4. As shown in the survey scan XPS spectra (Figure S2a), C 1s and N 1s peaks were observed for g-C_3N_4 and g-C_3N_4/$NaNbO_3$, while Na 1s, Nb 3d, and O 1s peaks were displayed for $NaNbO_3$ and g-C_3N_4/$NaNbO_3$. These characteristic peaks were undoubtedly consistent with chemical composition of the photocatalysts. As shown in the high resolution XPS spectra of C 1s (Figure S2b), as for g-C_3N_4, the two strong peaks located at 284.4 and 287.7 eV could be assigned to sp^2 C−C bonds and sp^2-bonded carbon in N-containing aromatic rings (N−C═N), respectively, which are considered the major carbon species in the g-C_3N_4.[52,53] The g-C_3N_4/$NaNbO_3$ composite displayed slightly lower binding energies of C 1s (284.3 and 287.6 eV) than that of pure g-C_3N_4, which was due to the fact that $NaNbO_3$ hybridized with g-C_3N_4 and thus led to the inner shift of C 1s. As shown in Figure S2c, the N 1s peaks located at 398.2 eV (g-C_3N_4) and 398.1 eV (g-C_3N_4/$NaNbO_3$) originated from C═N−C coordination.[54] In addition, the peak located at 1072.0 eV corresponded to the binding energy of Na 1s in $NaNbO_3$,[55] whereas the peak of g-C_3N_4/$NaNbO_3$ (1071.5 eV) was lower than that of pure $NaNbO_3$ (see Figure S 2d). Such a similar experimental phenomenon was also observed from the XPS spectra of Nb 3d (Figure S2e) and O 1s (Figure S 2f) peaks. That is, the binding energies of Nb $3d_{3/2}$ (209.1 eV), Nb $3d_{5/2}$ (206.6 eV), and O 1s (529.9 eV) of g-C_3N_4/$NaNbO_3$ were lower than those of Nb $3d_{3/2}$ (210.4 eV), Nb $3d_{5/2}$ (207.7 eV), and O 1s (530.6 eV) of pure $NaNbO_3$. XPS results implied the existence of chemical bonds in the g-C_3N_4/$NaNbO_3$ heterojunction.[56]

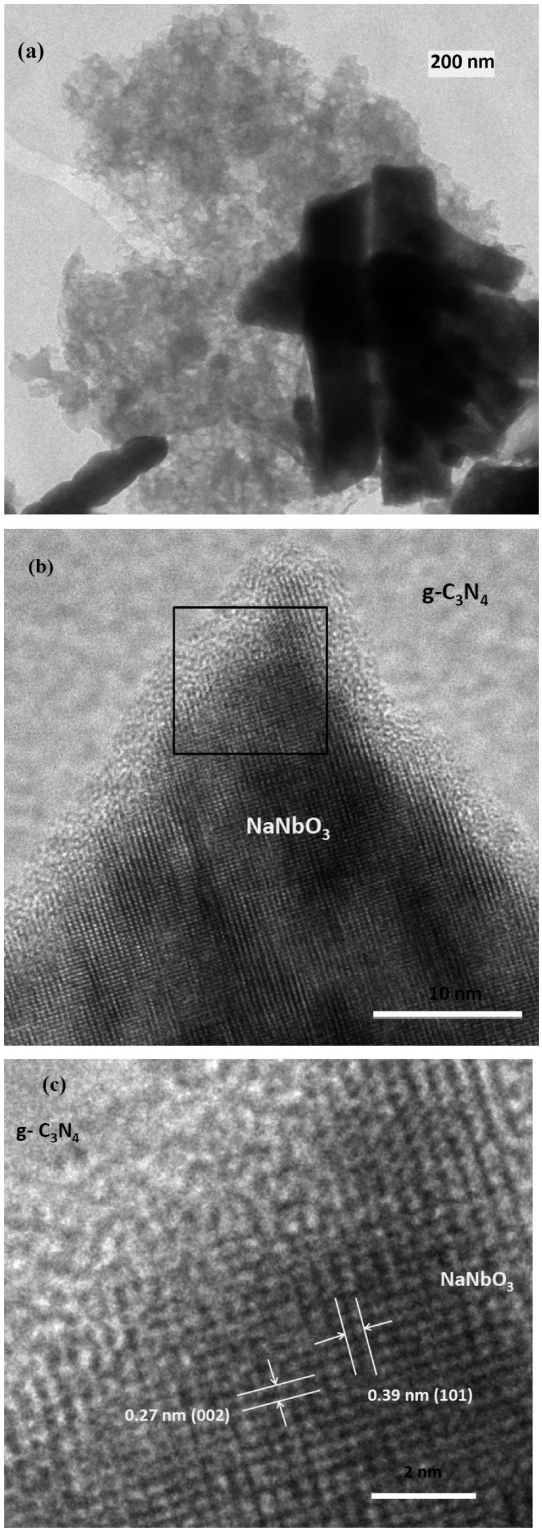

Figure 4. (a) TEM image and (b,c) high-magnification transmission electron microscopy (HRTEM) images of g-C_3N_4/$NaNbO_3$ heterojunction.

3.2. Photocatalytic Activity of g-C_3N_4/$NaNbO_3$ Heterojunction. In the present study, the CO_2 photoreduction experiments were carried out in the gaseous phase to evaluate the photocatalytic properties of as-prepared photocatalysts.

dx.doi.org/10.1021/cs500848f | ACS Catal. 2014, 4, 3637−3643

Figure 5 shows the CH_4 evolution rates over Pt loaded $NaNbO_3$, g-C_3N_4, and g-C_3N_4/$NaNbO_3$ composite photocatalysts and the BET surface areas. It was found that $NaNbO_3$ nanowires (12.0 m^2 g^{-1}) had a slightly larger surface area than g-C_3N_4 (6.5 m^2 g^{-1}). When g-C_3N_4 was introduced into $NaNbO_3$ nanowires, the surface area of g-C_3N_4–$NaNbO_3$ heterojunctions (10.7 m^2g^{-1}) was similar to that of $NaNbO_3$. During the first 4 h of irradiation, the rate of CH_4 generation over Pt-g-C_3N_4/$NaNbO_3$ was as high as 6.4 μmol h^{-1} g^{-1} in contrast to that of Pt-g-C_3N_4 (0.8 μmol h^{-1} g^{-1}). The heterojunction photocatalyst notably enhanced the photocatalytic performance compared with the naked photocatalyst. Namely, g-C_3N_4/$NaNbO_3$ improved over 8-fold higher activity than that of naked C_3N_4. In order to investigate the photocatalytic repeatability of the catalyst, the photocatalytic reduction of CO_2 over the used Pt-g-C_3N_4/$NaNbO_3$ sample was performed again. It was revealed that the photocatalytic activity of the used sample was similar to that of the fresh sample (see Figure S3). Figure 6 shows a comparison of the

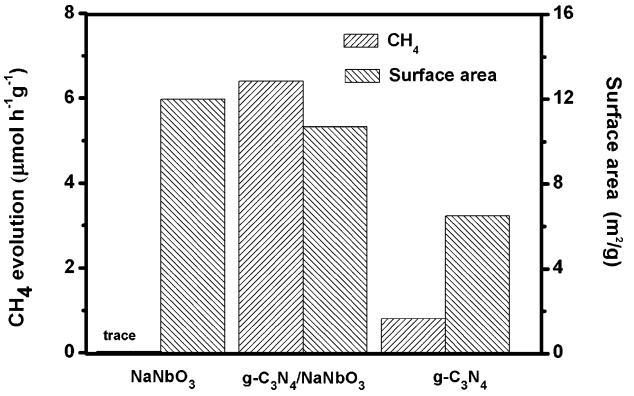

Figure 5. CH_4 evolution rates over Pt loaded $NaNbO_3$, g-C_3N_4, and g-C_3N_4/$NaNbO_3$ composite photocatalysts and the BET surface areas.

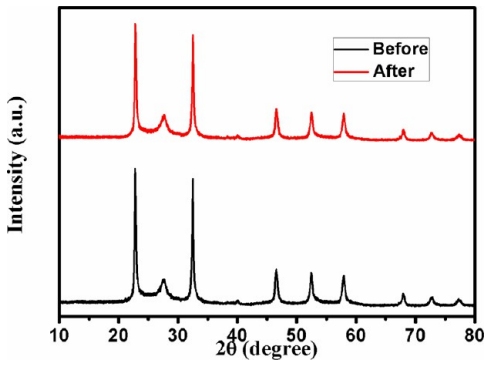

Figure 6. XRD patterns for Pt-g-C_3N_4/$NaNbO_3$ composite photocatalyst before and after photocatalytic reaction.

XRD patterns of pt-g-C_3N_4/$NaNbO_3$ before and after the photocatalytic reaction. There was no obvious peak change in the XRD patterns of pt-g-C_3N_4/$NaNbO_3$ before and after the photocatalytic reaction, indicating that the phase of the g-C_3N_4/$NaNbO_3$ catalyst was a stable photocatalyst without occurrence of structural degradation during the present photocatalytic reaction process.

3.3. Possible Photocatalytic Mechanism of g-C_3N_4/$NaNbO_3$ Heterojunctions. One can see that, although g-C_3N_4/$NaNbO_3$ and g-C_3N_4 have similar optical absorption and comparable surface areas, their photocatalytic activities in the photoreduction of CO_2 are apparently different. This implies that there should be another crucial factor that influences the photocatalytic activities notably. Actually, in addition to the optical absorption and surface area, the efficient charge separation of a semiconductor usually plays a crucial role in determining its photocatalytic property. Herein, band potentials of g-C_3N_4 and $NaNbO_3$ were investigated in order to clarify the charge separation in g-C_3N_4/$NaNbO_3$ interfaces.

The band edge positions of photocatalysts were theoretically speculated using the equation related to Mulliken electronegativity[57−60] and the band gap of a semiconductor, which is described by

$$E_{VB} = X - E_e + 0.5E_g \quad (1)$$

$$E_{CB} = E_{VB} - E_g \quad (2)$$

where E_{CB} and E_{VB} are the bottom conduction band (CB) and the top of the valence band (VB) relative to the normal hydrogen electrode (NHE) and E_g means the band gap energy of the photocatalyst, E_e is the energy of free electrons (4.5 eV), and X ($X = (X_1X_2X_3....X_n)^{1/n}$) is the geometric mean of the Mulliken electronegativity of the constituent atoms in the semiconductor. The Mulliken electronegativity of an atom is the arithmetic mean of the atomic electron affinity and the first ionization energy. Subsequently, E_{CB} of $NaNbO_3$ is determined to be −0.77 eV relative to the normal hydrogen electrode (NHE) in the view of the method inherent error (0.2 eV),[57] and the VB edge of $NaNbO_3$ is determined to be 2.63 eV from the band gap. The CB and VB edge potentials of g-C_3N_4 are determined to be −1.13 and 1.57 eV, respectively. In addition, the valence band X-ray photoelectron spectroscopy (VB-XPS) was further preformed to investigate the VB top of g-C_3N_4 and $NaNbO_3$. As shown in Figure 7, it could be seen that the

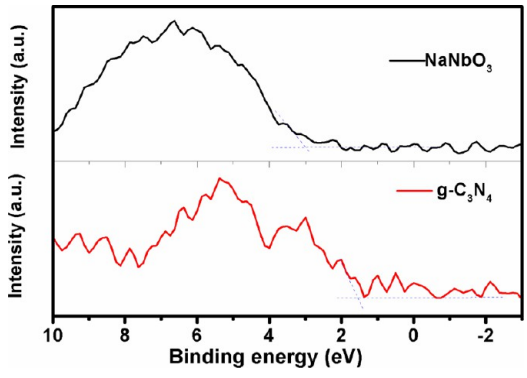

Figure 7. Valence band (VB) XPS spectra of g-C_3N_4 and $NaNbO_3$.

positions of the valence band edge of g-C_3N_4 and $NaNbO_3$ were located at ∼1.5 and 2.7 eV, respectively, which were consistent with the theoretical calculated results. Thus, it could be concluded that the VB top of $NaNbO_3$ is lower than that of g-C_3N_4, while the CB bottom of C_3N_4 is higher than that of $NaNbO_3$. On the basis of the above results and previous reports,[61−68] a possible mechanism for the enhanced photocatalytic activity over the present g-C_3N_4/$NaNbO_3$ is shown schematically in Figure 8. The g-C_3N_4 in the heterostructured photocatalysts acts as a sensitizer to absorb photons as well as excite electron and hole pairs upon light irradiation. Since the CB edge potential of g-C_3N_4 (−1.13 eV) is more negative than

dx.doi.org/10.1021/cs500848f | ACS Catal. 2014, 4, 3637−3643

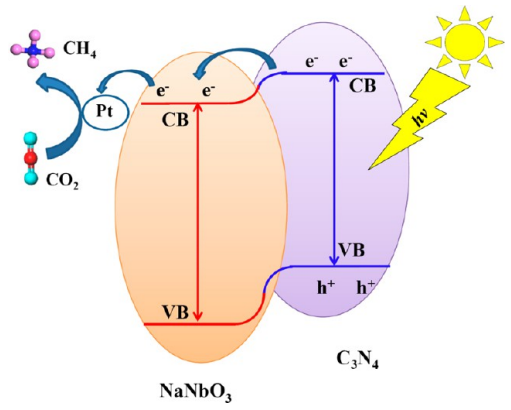

Figure 8. Schematic diagram of the separation and transfer of photogenerated charges in g-C_3N_4/$NaNbO_3$ composite under visible light irradiation.

that of $NaNbO_3$ (−0.77 eV), the photoexcited electrons on g-C_3N_4 could transfer to the CB of $NaNbO_3$. It is known that metallic noble metal Pt can serve as an excellent acceptor and trap for photoexcited electrons; hence the photoinduced electrons could be quickly transferred to the loaded Pt to generate CH_4. In such a way, the photoexcited electron−hole pairs could be effectively separated. Hence, the formed the junction between g-C_3N_4 and $NaNbO_3$ in the heterostructured photocatalysts would suppress the recombination of electrons and holes in carriers−transfer process and thus results in an enhanced photocatalytic activity of g-C_3N_4/$NaNbO_3$ heterojunctions. In order to obtain further insight into the band structures, density of states for $NaNbO_3$ and g-C_3N_4 were calculated using density functional theory (DFT). As shown in Figure S4, as for $NaNbO_3$, it was noted that the valence band (VB) edge was mainly composed of the O 2p orbital, while the conduction band (CB) edge was basically contributed by the Nb 4d orbital. The VB edge of g-C_3N_4 was basically made up of the N 2p orbital, while the CB edge consisted mainly of N 2p and C 2p orbitals.

In order to support above-proposed mechanism, we performed photoluminescence (PL) spectroscopy measurements to analyze the electron−hole pairs' recombination for g-C_3N_4 and g-C_3N_4/$NaNbO_3$. It is generally acknowledged that the higher fluorescence intensity means more recombination of electron−hole pairs and lower photocatalytic activities.[69] As shown in Figure 9, pure g-C_3N_4 excited at 350 nm had a main emission peak at about 460 nm, which was similar to the previous reports.[35,70] For g-C_3N_4/$NaNbO_3$, the emission intensity was much lower than that of pure g-C_3N_4 at a similar emission position, suggesting that the composites had a much lower recombination rate of photogenerated charge carriers. As mentioned above, it possibly originated from the charge transfer between g-C_3N_4 and $NaNbO_3$. In addition, the network structure of g-C_3N_4 could act as an excellent electron transport platform to facilitate the charge transfer process.[36,37] All these suggest some useful information to design an efficient photocatalysts for CO_2 reduction.

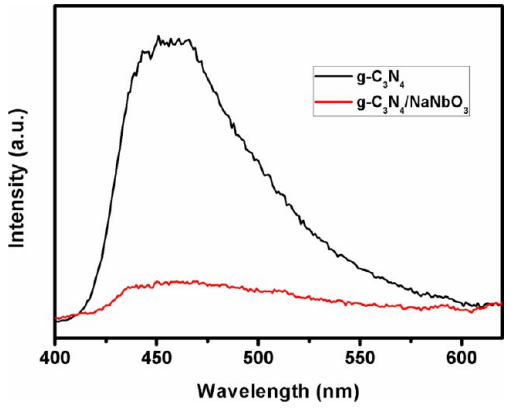

Figure 9. Photoluminescence (PL) spectra of g-C_3N_4 and g-C_3N_4/$NaNbO_3$ at an excitation wavelength of 350 nm.

4. CONCLUSION

In this study, we have successfully developed a visible-light-responsive g-C_3N_4/$NaNbO_3$ nanowire heterojunction photocatalyst via introducing polymeric g-C_3N_4 on $NaNbO_3$ nanowires. High-resolution transmission electron microscopy (HR-TEM) revealed that an intimate interface between C_3N_4 and $NaNbO_3$ nanowires formed in the heterojunctions. The resulting g-C_3N_4/$NaNbO_3$ nanowire heterojunctions owned strong absorption ability in the visible light region and had obviously enhanced photocatalytic activities for the CO_2 photoreduction. The photocatalytic activity of the g-C_3N_4/$NaNbO_3$ heterojunction for the CO_2 reduction was almost 8 times higher than that of individual C_3N_4 under visible light irradiation. Such a remarkable enhancement of photocatalytic activity was mainly attributed to the improved separation and transfer of photogenerated electron−hole pairs at the intimate interface of g-C_3N_4/$NaNbO_3$ heterojunctions, which could be ascribed to the well-aligned overlapping band structures of C_3N_4 and $NaNbO_3$. In summary, the present research is expected to be useful in development of new heterojunction photocatalysts and provide some meaningful information for photocatalytic CO_2 conversion.

■ ASSOCIATED CONTENT

Supporting Information

Typical SEM images and the corresponding energy dispersive spectra (EDS) pattern of g-C_3N_4/$NaNbO_3$ nanowires composite; XPS spectra of the $NaNbO_3$, g-C_3N_4, and g-C_3N_4/$NaNbO_3$; photocatalytic CH_4 evolution concentrations of Pt loaded g-C_3N_4/$NaNbO_3$ nanowires; density of states for g-C_3N_4 and $NaNbO_3$. This material is available free of charge via the Internet at http://pubs.acs.org.

■ AUTHOR INFORMATION

Corresponding Author

*E-mail: shihaifengnju@hotmail.com.

Notes

The authors declare no competing financial interest.

■ ACKNOWLEDGMENTS

The authors would like to acknowledge the financial support from National Natural Science Foundation of China (No 21203077).

■ REFERENCES

(1) Yang, H. Q.; Xu, Z. H.; Fan, M. H.; Gupta, R.; Slimane, R. B.; Bland, A. E.; Wright, I. *J. Environ. Sci.* **2008**, *20*, 14−27.
(2) Michl, J. *Nat. Chem.* **2011**, *3*, 268−269.
(3) Halmann, M. *Nature* **1978**, *275*, 115−116.
(4) Roy, S. C.; Varghese, O. K.; Paulose, M.; Grimes, G. A. *ACS Nano* **2010**, *4*, 1259−1278.

(5) Li, K. F.; An, X. Q.; Park, K. H.; Khraisheh, M.; Tang, J. W. *Cata Today* **2014**, *224*, 3−12.
(6) Kondratenko, E. V.; Mul, G.; Baltrusaitis, J.; Larrazabalc, G. O.; Amırez, P. J. R. *Energy Environ. Sci.* **2013**, *6*, 3112−3135.
(7) Navalón, S.; Dhakshinamoorthy, A.; lvaro, M.; Garcia, H. *ChemSusChem.* **2013**, *6*, 562−577.
(8) Varghese, O. K.; Paulose, M.; LaTempa, T. J.; Grimes, C. A. *Nano Lett.* **2009**, *9*, 731−737.
(9) Liang, Y. T.; Vijayan, B. K.; Lyandres, O.; Gray, K. A.; Hersam, M. C. *J. Phys. Chem. Lett.* **2012**, *3*, 1760−1765.
(10) Inoue, I.; Fujishima, A.; Konishi, S.; Honda, K. *Nature* **1979**, *277*, 637−638.
(11) W, N.; An, W. J.; Balavinayagam, R.; Mukherjee, S.; iedzwiedzki, D. M.; Gangopadhyay, S.; Biswas, P. *J. Am. Chem. Soc.* **2012**, *134*, 11276−11281.
(12) Liu, L. J.; Zhao, H. L.; Andino, J. M.; Li, Y. *ACS Catal.* **2012**, *2*, 1817−1828.
(13) Singh, V.; Ignacio, J. C. B.; Josep, C. R.; Prashant, N. *Nano Lett.* **2014**, *14*, 597−603.
(14) Hoffmann, M. R.; Moss, J. A.; Baum, M. M. *Dalton Trans.* **2011**, *40*, 5151−5158.
(15) In, S. I.; Vaughn, D. D.; Schaak, R. E. *Angew. Chem., Int. Ed.* **2012**, *51*, 3915−3918.
(16) Yan, S. C.; Ouyang, S. X.; Gao, J.; Yang, M.; Feng, J. Y.; Fan, X. X.; Wan, L. J.; Li, Z. S.; Ye, J. H.; Zhou, Y.; Zou, Z. G. *Angew. Chem., Int. Ed.* **2010**, *49*, 6400−6404.
(17) Iizuka, K.; Wato, T.; Miseki, Y.; Saito, K.; Kudo, A. *J. Am. Chem. Soc.* **2011**, *133*, 20863−20868.
(18) Xi, G. C.; Ouyang, S. X.; Li, P.; Ye, J. H.; Ma, Q.; Su, N.; Bai, H.; Wang, C. *Angew. Chem., Int. Ed.* **2012**, *51*, 2395−2399.
(19) Severin, N. H.; Lukas, S. M.; Jacek, K. S. *Angew. Chem., Int. Ed.* **2013**, *52*, 7372−7408.
(20) Kazuhiko, M.; Lu, D. L.; Domen, K. *Angew. Chem., Int. Ed.* **2013**, *52*, 6488−6491.
(21) Liu, Q.; Zhou, Y.; Kou, J.; Chen, X.; Tian, Z.; Gao, J.; Yan, S.; Zou, Z. G. *J. Am. Chem. Soc.* **2010**, *132*, 14385−14387.
(22) Zhang, N.; Ouyang, S. X.; Kako, T.; Ye, J. H. *Chem. Commun.* **2012**, *48*, 1269−1271.
(23) Mori, K.; Yamashita, H.; Anpo, M. *RSC Adv.* **2012**, *2*, 3165−3172.
(24) Dhakshinamoorthy, A.; Navalon, S.; Corma, A.; Garcia, H. *Energy Environ. Sci.* **2012**, *5*, 9217−9233.
(25) Gordon, T. R.; Cargnello, M.; Paik, T.; Mangolini, F.; Weber, R. T.; Fornasiero, P.; Murray, C. B. *J. Am. Chem. Soc.* **2012**, *134*, 6751−6761.
(26) Yang, S. B.; Gong, Y. J.; Zhang, J. S.; Zhan, L.; Ma, L. L.; Fang, Z. Y.; Vajtai, R.; Wang, C. X.; Pulickel, M. A. *Adv. Mater.* **2013**, *25*, 2452−2456.
(27) Maeda, X.; Wang, Y.; Nishihara, D.; Lu, A.; Antonietti, M.; Domen, K. *J. Phys. Chem. C* **2009**, *113*, 4940−4947.
(28) Wang, K.; Maeda, X.; Chen, K.; Takanabe, K.; Domen, Y.; Hou, X. F.; Antonietti, M. *J. Am. Chem. Soc.* **2009**, *131*, 1680−1681.
(29) Ding, Z.; Chen, X.; Antonietti, M.; Wang, X. *ChemSusChem* **2011**, *4*, 274−281.
(30) Yan, S. C.; Li, Z. S.; Zou, Z. G. *Langmuir* **2009**, *25*, 10397−10401.
(31) Dong, G. H.; Zhang, L. Z. *J. Mater. Chem.* **2012**, *22*, 1160−1166.
(32) Mao, J.; Peng, T. Y.; Zhang, X. H.; Li, K.; Ye, L. Q.; Zan, L. *Catal. Sci. Technol.* **2013**, *3*, 1253−1260.
(33) Wang, X.; Maeda, A.; Thomas, K.; Takanabe, G.; Xin, J. M.; Carlsson, K.; Domen, K.; Antonietti, M. *Nat. Mater.* **2009**, *8*, 76−80.
(34) Yan, S. C.; Lv, S. B.; Li, Z. S.; Zou, Z. G. *Dalton Trans.* **2010**, *39*, 1488−1491.
(35) Sun, L. M.; Zhao, X.; Jia, C. J.; Zhou, Y. X.; Cheng, X. F.; Li, P.; Liu, L.; Fan, W. L. *J. Mater. Chem.* **2012**, *22*, 23428−23438.
(36) Wang, Y. J.; Shi, R.; Lin, J.; Zhu, Y. F. *Energy Environ. Sci.* **2011**, *4*, 2922−2929.
(37) Pan, C. S.; Xu, J.; Wang, Y. J.; Li, D.; Zhu, Y. F. *Adv. Funct. Mater.* **2012**, *22*, 1518−1524.
(38) Zhang, J. Y.; Wang, Y. H.; Jin, J.; Zhang, J.; Lin, Z.; Huang, F.; Yu, J. G. *ACS Appl. Mater. Interfaces* **2013**, *5*, 10317−10324.
(39) Ge, L.; Han, C. C.; Liu, J. *Appl. Catal. B Environ* **2011**, *108−109*, 100−107.
(40) Yang, N.; Li, G. Q.; Wang, W. L.; Yang, X. L.; Zhang, W. F. *J. Phys. Chem. Solids* **2011**, *72*, 1319−1324.
(41) Li, G. Q.; Yang, N.; Wang, W. L.; Yang, W. F. *J. Phys. Chem. C* **2009**, *113*, 14829−14833.
(42) Yuan, Y. P.; Cao, S. W.; Liao, Y. S.; Yin, L. S.; Xue, C. *Appl. Catal. B Environ.* **2013**, *140−141*, 164−168.
(43) Cao, S. W.; Liu, X. F.; Yuan, Y. P.; Zhang, Z. Y.; Liao, Y. S.; Fang, J.; Say, C. J. L.; Sum, T. C.; Xue, C. *Appl. Catal. B Environ.* **2014**, *147*, 940−946.
(44) Shi, H. F.; Li, X. K.; Wang, D. F.; Yuan, Y. P.; Zou, Z. G.; Ye, J. H. *Catal. Lett.* **2009**, *132*, 205−212.
(45) Saito, K.; Kudo, A. *Inorg. Chem.* **2010**, *49*, 2017−2019.
(46) Shi, H. F.; Wang, T. Z.; Chen, J.; Zhu, C.; Ye, J. H.; Zou, Z. G. *Catal. Lett.* **2011**, *141*, 525−530.
(47) Li, P.; Xu, H.; Liu, L.; Kako, T.; Umezawa, N.; Abe, H.; Ye, J. *J. Mater. Chem. A* **2014**, *2*, 5606−5609.
(48) Shi, H. F.; Zou, Z. G. *J. Phys. Chem. Solids* **2012**, *73*, 788−792.
(49) Li, G. Q.; Yi, Z. G.; Bai, Y.; Zhang, W. F.; Zhang, H. T. *Dalton Trans.* **2012**, *41*, 10194−10198.
(50) Wang, D. F.; Pierre, A.; Kibria, M. G.; Cui, K.; Han, X. G.; Bevan, K. H.; Guo, H.; Paradis, S.; Hakima, A. R.; Mi, Z. T. *Nano Lett.* **2011**, *11*, 2353−2357.
(51) Zhou, H. L.; Qu, Y. Q.; Zeid, T.; Duan, X. F. *Energy Environ. Sci.* **2012**, *5*, 6732−6743.
(52) Wang, Y.; Wang, X.; Antonietti, M. *Angew. Chem., Int. Ed.* **2012**, *51*, 68−89.
(53) Vinu, A. *Adv. Funct. Mater.* **2008**, *18*, 816−827.
(54) Xiang, Q. J.; Yu, J. G.; Jaroniec, M. *J. Phys. Chem. C* **2011**, *115*, 7355−7363.
(55) Magdalena, K.; Ewa, T.; Antoni, K. *Solid State Commun.* **2006**, *137*, 469−473.
(56) Sun, J. X.; Yuan, Y. P.; Qiu, L. G.; Jiang, X.; Xie, A. J.; Shen, Y. H.; Zhu, J. F. *Dalton Trans.* **2012**, *41*, 6756−6763.
(57) Nethercot, A. H. *Phys. Rev. Lett.* **1974**, *33*, 1088.
(58) Butler, M. A.; Ginley, D. S. *J. Electrochem. Soc.* **1978**, *125*, 228.
(59) Shi, H.; Li, Z.; Kou, J.; Ye, J.; Zou, Z. *J. Phys. Chem. C* **2011**, *115*, 145−151.
(60) Shi, H. F.; Chen, G. Q.; Zou, Z. G. *Appl. Catal. B Environ.* **2014**, *156−157*, 378−384.
(61) Wang, X. C.; Blechert, S.; Antonietti, M. *ACS Catal.* **2012**, *2*, 1596−1606.
(62) Marschall, R. *Adv. Funct. Mater.* **2014**, *24*, 2421−2440.
(63) Li, K.; Chai, B.; Peng, T.; Mao, J.; Zan, L. *ACS Catal.* **2013**, *3*, 170−177.
(64) Xu, H.; Yan, J.; Xu, Y.; Song, Y.; Li, H.; Xia, J.; Huang, C.; Wan, H. *Appl. Catal. B Environ.* **2013**, *129*, 182−193.
(65) Kumar, A.; Surendar, T.; Baruah, A.; Shanker, V. *J. Mater. Chem. A* **2013**, *1*, 5333−5340.
(66) Cao, S.; Yu, J. *J. Phys. Chem. Lett.* **2014**, *5*, 2101−2107.
(67) Guan, X. J.; Guo, L. J. *ACS Catal.* **2014**, *4*, 3020−3026.
(68) Kumar, S.; Khanchandani, S.; Thirumal, M.; Ganguli, A. K. *ACS Appl. Mater. Interfaces* **2014**, DOI: 10.1021/am503055n.
(69) Hoffmann, M. R.; Martin, S. T.; Choi, W. Y.; Bahnemann, D. W. *Chem. Rev.* **1995**, *95*, 69−96.
(70) Zhang, X. H.; Yu, L. J.; Zhuang, C. S.; Peng, T. Y.; Li, R. J.; Li, X. J. *ACS Catal.* **2014**, *4*, 162−170.